The Abdus Salam
International Centre for Theoretical Physics

United Nations
Educational, Scientific and
Cultural Organization

IAEA
International Atomic Energy Agency

2060-32

Advanced School on Non-linear Dynamics and Earthquake Prediction

28 September - 10 October, 2009

Recurrence pattern of Holocene earthquakes along the Dead Sea transform revealed by varve-counting and radiocarbon dating of lacustrine sediments

Amotz Agnon
Institute of Earth Sciences Hebrew University
Jerusalem
Israel

Available online at www.sciencedirect.com
SCIENCE DIRECT®
Earth and Planetary Science Letters 222 (2004) 301–314
EPSL
www.elsevier.com/locate/epsl

Recurrence pattern of Holocene earthquakes along the Dead Sea transform revealed by varve-counting and radiocarbon dating of lacustrine sediments

Claudia Migowski[a,*], Amotz Agnon[b,1], Revital Bookman[b,c,2], Jörg F.W. Negendank[a,3], Mordechai Stein[b,c,4]

[a] *GeoForschungsZentrum Potsdam, Sec. 3.3 Climate Dynamics and Sediments, Telegrafenberg, D-14473 Potsdam, Germany*
[b] *Institute of Earth Sciences, The Hebrew University of Jerusalem, Givat Ram, 91904 Jerusalem, Israel*
[c] *Geological Survey of Israel, Malkhei Yisrael 30 St., Jerusalem, Israel*

Received 10 July 2003; received in revised form 11 February 2004; accepted 14 February 2004

Abstract

A high-resolution Holocene seismic history of the Dead Sea Transform (DST) is established from laminated sedimentary cores recovered at the shores of the Dead Sea. Radiocarbon dating and annual laminae counting yield excellent agreement between disturbed sedimentary structures (identified as seismites) and the historical earthquake record: All recent and historical strong events of the area were identified, including the major earthquakes of A.D. 1927, 1837, 1212, 1033, 749, and 31 B.C. The total of 53 seismites recognized along the entire Holocene profile indicate varying recurrence intervals of seismic activity between a few and 1000 years, with a conspicuous minimum rate at 2100–31 B.C. and a noticeable maximum during the past six to eight centuries. Most of the epicenters of the correlated earthquakes are situated very close to the Dead Sea (within 150 km) or up to 400 km north of it along the DST. Between 1000 B.C. and A.D. 1063, and from A.D. 1600 to recent time the epicenters are all located on the northern segment of the DST, whereas prior to 1000 B.C. and between A.D. 1000 and 1600 they appear to scatter along several segments of the DST. We establish how the local intensity exerts a control on the formation of seismites. At historically estimated intensities greater than VII, all well documented earthquakes are correlated, whereas at intensities smaller than VI none are matching.

The periods with enhanced earthquake rate along the DST correlate with those along the North Anatolian Fault as opposed to the intervening East Anatolian Fault. This may indicate some elastic coupling on plate-boundary scale that may also underlie escape and extrusion tectonics, typical of continental collision.

Keywords: paleoseismology; earthquakes; Dead Sea Transform; Holocene sediments; varves; seismite; active faulting; recurrence interval; Anatolian block; lateral extrusion

* Corresponding author. Tel.: +49-331-288-1381; fax: +49-331-288-1302.
E-mail addresses: migo@gfz-potsdam.de (C. Migowski), amotz@huji.ac.il (A. Agnon), revital@vms.huji.ac.il (R. Bookman), neg@gfz-potsdam.de (J.F.W. Negendank), motis@vms.huji.ac.il (M. Stein).
[1] Tel.: +972-2-6584743; fax: +972-2-5662581.
[2] Tel.: +972-2-6584272; fax: +972-2-5662581.
[3] Tel.: +49-331-288-1300; fax: +49-331-288-1302.
[4] Tel.: +972-2-65314296; fax: +972-2-5662581.

0012-821X/$ - see front matter © 2004 Elsevier B.V. All rights reserved.
doi:10.1016/j.epsl.2004.02.015

1. Introduction

The Dead Sea Transform (DST), which separates the Arabian and Sinai plates [1,2] (Fig. 1A), has been the locus of tectonic and seismic activity over timescales of several million years to historical periods [2–4]. A long-standing problem in the tectonic reconstruction of the DST is the apparent gap between the long-term rate of plate movement along the major faults and the seismic moment release [5]. This gap possibly indicates that the seismic activity is not uniform on a historical time scale, with alternating periods of activity and quiescence [6,7]. More recent estimates of the long-term rate [2,8] and geodetic measurements of the current rate [1,9] confirm the gap with modern estimates of the seismic moment release [10]. The temporal alternation between activity and quiescence may be associated with spatial migration of activity between adjacent plate boundaries, as shown for the North and East Anatolian Fault systems [3]. An assessment of this notion requires detailed knowledge on the temporal occurrence of the earthquakes, with constraints on rupture area and magnitudes.

In the present study we examine the spatial and temporal distribution of earthquakes that occurred along the Dead Sea Transform (DST) during the Holocene period. The human development in the Dead Sea basin and the Jordan Valley reflects to a large extent the climatic and tectonic histories. As this region was the locus of human settlement since the early Pleistocene [11], rich historical documentation of earthquake activity is available for the past 2800 years [12–15], allowing for comparison with the geological evidence of paleo-earthquakes. This evidence appears as disturbances in geological sections of lacustrine sediments that were deposited in the Dead Sea basin during the Holocene. The sedimentary section at the Ze'elim gully (Figs. 1B and 2) exposes disturbed sedimentary structures that were correlated with the historical earthquakes of the region [16]. Nevertheless, the exposed Ze'elim section reveals only parts of the Holocene paleo-seismic record because it is located on a terrace, elevated relatively to the level of the Dead Sea during much of the late Holocene [17]. The location of the Ze'elim terrace is sensitive to lake level fluctuations that induced hiatuses during low lake stands. In the Ze'elim record several of the missing major earthquakes lie indeed in periods of low lake stands and sedimentary hiatuses [16,17].

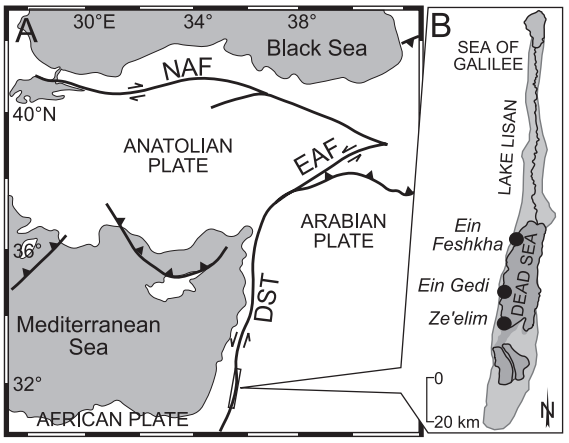

Fig. 1. (A) Map of major tectonic boundaries and plate motions in the Eastern Mediterranean region [1]. The heavy arrow indicates the convergence vector of the northern Arabian plate; NAF—North Anatolian Fault; EAF—East Anatolian Fault; DST—Dead Sea Transform. (B) Drilling sites along the Dead Sea shore and the Ze'elim outcrop are shown.

In the present study, we extracted sediment cores at different sites of recently emerged shorelines (Fig. 1B). These cores recovered sedimentary sections that represent the deeper lacustrine environment of the Holocene Dead Sea. The Ein Gedi site is less sensitive to lake level changes and therefore should contain a continuous depositional and seismite sequence. We anticipated finding in the Ein Gedi core the "missing seismites" from earthquakes that correspond to hiatuses in the Ze'elim section, thus completing the entire historical record. This would provide a crucial test for the assessment of the disturbed sedimentary structures as seismites. The Ein Gedi core penetrated 21 m beneath the 1997 surface of the Dead Sea shore (at 413 m below mean sea level) reaching at its bottom a thick salt layer (Fig. 2), which marks the base of the Holocene at several sites in the region [18]. Thus, the Ein Gedi core comprises the entire Holocene period. Another core representing the lacustrine environment was recovered in the Ein Feshkha site on the north-western side of the Dead Sea (Fig. 1B) and its record is used for comparison with the Ein Gedi core. In addition, we

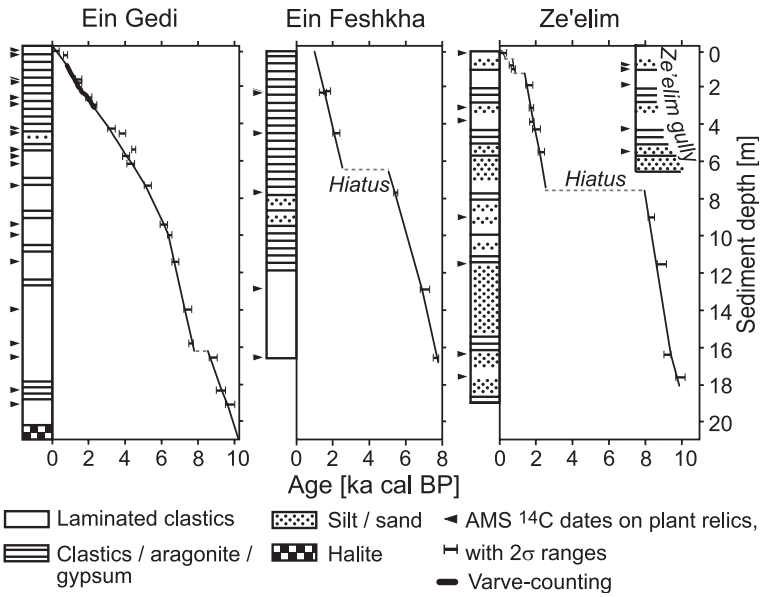

Fig. 2. Lithology of the sediment cores and the established age-depth models of the different profiles. The Ze'elim coring profile is paralleled by the Ze'elim gully wall [16]. The Ein Gedi chronology is based on 20 radiocarbon dates and on the varve counted section (black line) in the upper part.

recovered a core next to the exposed section of the Ze'elim gully, which allows us to compare the sedimentary record in a lake versus a nearshore environment. (Figs. 1B and 2).

2. The lithology and chronology of the cores

Textural and mineralogical properties of the cores were examined in thin sections under microscopic binocular. The thin sections were further used for laminae counting.

The Ein Gedi core typically comprises laminated clay-sized clastic sediments and authigenic aragonite and gypsum. The laminae are 0.2–2 mm in thickness, and the petrographic examination reveals clastic laminae, often alternating in couplets with aragonite, or appear as triplets of clastic detritus, aragonite and gypsum. The clastic material was brought into the lake by seasonal floods; the aragonite laminae precipitate from the upper surface water layer of the lake following the supply of bi-carbonate to the lake [19] by the floods from the Jordan river. The gypsum laminae may represent drier years when the upper water mass is diminished due to lower water input and enhanced evaporation [19]. Between 10.5 and 16 m sediment depth, the Ein Gedi core mainly consists of the clastic component with sparse formation of pure aragonite laminae, presumably because of a dry climate (Fig. 2).

Radiocarbon dating combined with laminae counting allows constraining the absolute sedimentation rate of the profile (Fig. 2). Along the entire Ein Gedi profile, 20 wood fragments washed in by floods have been AMS radiocarbon dated (Table 1, calibration according to Ref. [20]). Additionally, the laminae in the uppermost part of the profile were counted under the microscope, and their thickness measured. With that, we obtained a floating chronology of 1500 counted years between 0.78 and 3.02 m sediment depth, in a range of ~700–2200 years ago. Within the errors of radiocarbon dating, the clastic-aragonite couplets and clastic-aragonite-gypsum triplets can be defined as annual deposits, namely they are varves. A similar conclusion was reached for the alternating clastic-aragonite couplets in the late Pleistocene Lisan Formation [21]. The working hypothesis that the laminae are varves enabled us to establish an accurate

Table 1
AMS Radiocarbon dates from the Ein Gedi site

	Lab. No.	Depth (m)	^{14}C age (a BP)	Calibrated ^{14}C age 2σ (a cal A.D./B.C.)	Most probable ages (A.D./B.C.)	Shift of the curve from 2σ ranges (a)
1	KIA11626	0.02	160 ± 33	A.D. 1660–1889 A.D. 1910–1950	A.D. 1840–1850	0[a]
2	KIA5841	0.22	800 ± 30	A.D. 1189–1204 A.D. 1205–1282	A.D. 1700–1712	>418[a] recycled material?
3	KIA11627	1.58	1528 ± 39	A.D. 427–623 A.D. 630–637	A.D. 936–942	>299[b]
4	KIA9122	1.70	1555 ± 30	A.D. 426–599	A.D. 854–860	>255[b]
5	KIA5842	2.50	2070 ± 30	171–16 B.C. 13 B.C.–A.D.1	A.D. 275–283	>274[b]
6	KIA11628	2.86	2293 ± 29	400–356 B.C. 286–256 B.C. 243–233 B.C.	31–75 B.C.	>158[b]
7	KIA11629	4.16	3065 ± 40	1426–1417 B.C. 1413–1255 B.C. 1240–1212 B.C. 1196–1193 B.C. 1135–1133 B.C.	1310 B.C.	0[a]
8	KIA9123	4.47	3545 ± 35	2005–2003 B.C. 1953–1766 B.C. 1759–1750 B.C.	1365–1570 B.C.	>180[a]
9	KIA11630	5.35	4018 ± 31	2618–2609 B.C. 2596–2590 B.C. 2582–2465 B.C.	2050–2100 B.C.	>365[a]
10	KIA5843	5.70	3680 ± 30	2184–2183 B.C. 2140–2005 B.C. 2004–1955 B.C.	2150–2184 B.C.	0[a]
11	KIA11631	6.08	3836 ± 40	2459–2194 B.C. 2173–2142 B.C.	2450–2459 B.C.	0[a]
12	KIA11632	7.28	4546 ± 32	3366–3262 B.C. 3239–3165 B.C. 3163–3099 B.C.	3300–3367 B.C.	0[a]
13	KIA5844	9.42	5280 ± 40	4224–3980 B.C.	4230 B.C.	–
14	KIA11633	10.00	5595 ± 34	4495–4468 B.C. 4463–4348 B.C.	4450 B.C.	–
15	KIA5845	11.44	5900 ± 40	4897–4891 B.C. 4876–4873 B.C. 4849–4816 B.C. 4812–4690 B.C.	4800 B.C.	–
16	KIA5846	14.01	6460 ± 70	5555–5553 B.C. 5533–5302 B.C.	5400 B.C.	–
17	KIA5847	15.88	6730 ± 40	5721–5612 B.C. 5586–5559 B.C.	5660 B.C.	–
18	KIA11634	16.65	7874 ± 39	7026–7019 B.C. 6999–6989 B.C. 6982–6967 B.C. 6948–6933 B.C. 6914–6881 B.C. 6828–6638 B.C. 6617–6610 B.C.	6610 B.C.	–

Table 1 (*continued*)

	Lab. No.	Depth (m)	^{14}C age (a BP)	Calibrated ^{14}C age 2σ (a cal A.D./B.C.)	Most probable ages (A.D./B.C.)	Shift of the curve from 2σ ranges (a)
19	KIA5848	18.40	8200 ± 40	7446–7437 B.C. 7418–7411 B.C. 7396–7393 B.C. 7347–7076 B.C.	7150 B.C.	–
20	KIA11635	19.17	8644 ± 88	7959–7950 B.C. 7943–7925 B.C. 7924–7539 B.C.	7700 B.C.	–

Calibration according to [20].

[a] Shift from radiocarbon dates to proposed ages according to earthquake correlation.

[b] Shift from radiocarbon dates to proposed ages according to earthquake correlation and varve counting.

age-depth model, encompassing the last 10,000 years (Fig. 2).

3. Development of a seismite chronology in the Dead Sea sediments

The first earthquake records in the Dead Sea region, using a sedimentary inventory [7,22], were established from sediments of late Pleistocene Lake Lisan. The Lisan Formation comprises sequences of alternating laminae of authigenic aragonite and silty detritus deposited during enhanced freshwater input to the lake and sequences of sands and silts deposited during low lake stands [16,23,24]. This sedimentary pattern is punctuated by sequences with disturbed sedimentary structures that typically consist of aragonite fragments ‘‘floating’’ in silty detrital matrix (similar to those illustrated in Fig. 3) without any indication of transport effect. Several sedimentary structures could be associated with liquefaction and earthquake activity [7], thus leading to the interpretation of the disturbed layers as being seismites. Moreover, the disturbed sedimentary structures in the Lisan Formation were found in direct association with syndepositional surface fault ruptures, lending strong support to the seismite interpretation [25]. Marco et al. [7,25] suggested that the original laminae were deformed during earthquakes at the water–sediment interface. The sediments were fluidized, brecciated, re-suspended, and then re-settled in their present deformed sedimentary structure. The timing of each event is constrained by dating the first undisturbed layer overlying the disturbed sequence. The temporal distribution of the seismites in the Lisan section was determined by U-series dating obtained on adjacent aragonite laminae [26]. It was found that intervals of approximately 10,000 years of seismic activity alternate with a similar time span of quiescence [7]. The Lisan study was followed by the identification of similar sedimentary disturbances in the exposed section of the upper Holocene Dead Sea in the Ze’elim gully [16]. There, the ages of the seismites were determined by radiocarbon dating of organic remains found within the seismites or in adjacent layers.

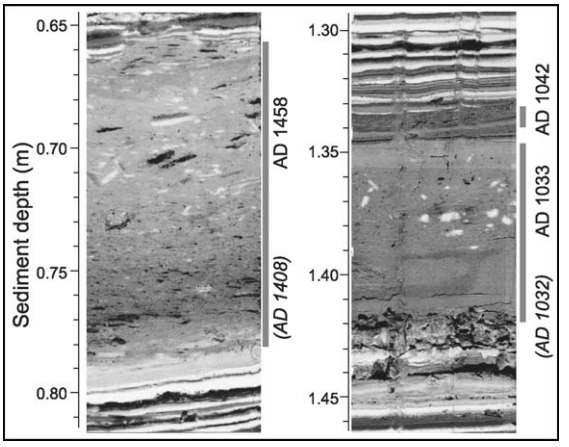

Fig. 3. Two typical examples of disturbed sediment sequences in the Ein Gedi profile: The sequence between 0.65 and 0.78 m core depth is correlated with the earthquake of A.D. 1458, whereas the earlier event of the year A.D. 1408 is masked in the sequence (left). The sequence between 1.35 and 1.42 m depth is identified as being created during the earthquake of A.D. 1033 (right).

Table 2
Deformed sequences of the Ein Gedi site and their correlation with earthquakes

No.	Depth (m)	Thickness (cm)	Type-I, -II, -III	Date (A.D./B.C.)	Magnitude	Sources
1	− 0.13[a]	10	I	A.D. 1927	6.3	[12,13,15, 16,29]
2	0.03	3	II	A.D. 1837	7.4	[13,15,27]
			masked	A.D. 1834	6.4	[13,16]
3	0.08	3	II	A.D. 1822	7.6	[13,15,27]
4	0.22	2	II	A.D. 1759	7.4	[13,27,30]
5	0.27	12	I	A.D. 1712	5.5	[13]
6	0.41	4.8	II	A.D. 1656	7.1	[13,15]
7	0.52	1	II	A.D. 1588	6.7	[12,15]
8	0.56	3	II	A.D. 1546	6.1	[12,15,16]
9	0.66	13	I	A.D. 1458	6.5	[12,13,16]
			masked	A.D. 1408	>7.5	[15,30]
Counted interval			–	*A.D. 1303*	*8.0*	[12,15]
10	0.9481	1	II	A.D. 1293	6.6	[12,13,16]
11	1.0307	4.2	II	A.D. 1212	6.7	[12,13,16]
			masked	*A.D. 1202*	*7.5*	[12,13,15, 27,28,30]
			–	*A.D. 1170*	*7.5*	[12,15,30]
			–	*A.D. 1157*	*7–7.5*	[15,30]
			–	*A.D. 1139*	*7.4*	[15]
12	1.23	0.8	III	A.D. 1114	7.9	[13,15,27]
13	1.32	0.4	III	A.D. 1068	6.9	[13,15,16,27]
			masked	*A.D. 1063*	*6.5–7*	[13]
14	1.34	0.8	III	A.D. 1042	7.3	[15]
15	1.3531	7.4	I	A.D. 1033	7.1	[4,12,13,15, 16,27]
			masked	*A.D. 1032*	*6.9*	[13,15]
16	1.495	0.2	III	A.D. 991	6.7	[15]
17	1.698	0.8	III	A.D. 859	7–7.5	[15]
18	1.9207	0.2	III	A.D. 749	7–7.5	[4,12–16,30]
19	1.99	0.5	III	A.D. 660	>6.0	[13,14]
20	2.2033	0.3	III	A.D. 551	7.5	[4,12,13, 15,16]
21	2.2991	0.7	III	A.D. 502	7.0	[13,15]
			masked	*A.D. 500*	*7.8*	[13,15]
22	2.3716	0.5	III	A.D. 419	6.9	[13,14]
			–	*A.D. 363*	*6.7*	[13–16]
			–	*A.D. 349*	*7.0*	[15]
			–	*A.D. 306*	*7.1*	[13,15]
23	2.5562	0.66	III	*~ A.D. 175*	–	–
24	2.6497	0.2	III	A.D. 115	7.4	[13,15]
25	2.6565	0.5	III	A.D. 112	6.2	[12]
26	2.6645	0.5	III	*~ A.D. 90*	–	–
27	2.6820	0.4	III	A.D. 76	7.0	[15]
28	2.7420	0.2	III	A.D. 33	5.5	[13,16]
			–	*A.D. 19*	*6.8*	[13,15]
29	2.8386	9	I	31 B.C.	6.7	[13–16]
			masked	*64 B.C.*	*7.7*	[13,15,16]
30	2.9493	1	II	92 B.C.	7.1	[13,15]
31	3.0248	1	II	140 B.C.	7.0	[15]
			masked	*148 B.C.*		[15]
32	3.41	1	II	525 B.C.	7.5	[15]

Table 2 (*continued*)

No.	Depth (m)	Thickness (cm)	Type-I, -II, -III	Date (A.D./B.C.)	Magnitude	Sources
33	3.51	2	II	*~ 700 B.C.*	–	–
34	3.55	5	I	759 B.C.	7.3	[4,15]
35	3.79	5	I	ca. 1050 B.C.	7.0	[15]
36	*3.81*	*1*	*II*	*~ 1100 B.C.*	–	–
37	4.3	7	I	ca. 1365 B.C.	7.8	[15]
38	4.52	3	II	ca. 1560 B.C.	6.8	[15]
39	4.62	11	I	*~ 1800 B.C.*	–	–
40	5.05	7	I	*~ 2000 B.C.*	–	–
41	5.36	9	I	ca. 2050 B.C.	8 ?	[15]
42	5.61	7	I	ca. 2100 B.C.	6.8	[15]
43	6.42	7	I	ca. 2700 B.C.	>6.3 ?	[4]
44	7.2	2	II	33–3600 B.C.	>6.0 ?	[15]
45	8.33	6	I	4000 B.C.	>6.2 ?	[4]
46	8.42	4	II	*~ 4200 B.C.*	–	–
47	10.19	3	II	*~ 4450 B.C.*	–	–
48	10.76	2	II	*~ 4600 B.C.*	–	–
49	15.80	14	I	*~ 5600 B.C.*	–	–
50	16.45	4	II	*~ 6000 B.C.*	–	–
51	17.27	13	I	*~ 6500 B.C.*	–	–
52	17.45	4	II	*~ 6600 B.C.*	–	–
53	17.96	2	II	*~ 6800 B.C.*	–	–

[a] Depth is a sub-bottom depth of the 21 m long core. Negative depth results from the profile extension by the additional 30 cm short complementary top-core.

The Ein Gedi core provides a continuous record including 53 deformed layers that resemble the disturbed sequences of the Lisan Formation, thus are identified as seismites (Table 2). The ages of the seismites were determined by radiocarbon dating, and were further incorporated within the counting age-depth calendar model. The floating annual chronology was finally fitted by the correlation to the historical strong earthquake record from the Dead Sea area (Fig. 4). The counting curve between 0.78 and 3.03 m, was first matched within the two sigma ranges of the radiocarbon dates. The gradients of both are in good agreement. In the next step the top of each disturbed sequence in the curve was matched to one of the documented earthquake dates by shifting the curve on the time-axis. This process was iterated searching for a satisfactory match for the entire section. Due to the non-repetitive character of both historic and sedimentary record there is a single choice of match for which the congruence is significantly better than all the others (Fig. 4). Account had to be taken for magnitude and epicentral distance: earthquakes creating a disturbed sequence in the Dead Sea need to be sufficiently strong, and also their epicenter should be sufficiently close. The distance-magnitude plot (Fig. 5) of the available earthquake data [4,10–16,27–31] is a tool for choosing among different events.

Within the counting interval of 1500 years, 27 historical earthquakes from the Dead Sea region can be matched with the age-depth counting model. Twenty-one of these events are correlated to the top of deformed layers and six are masked by subsequent deformation (Table 2). This finding is significant since the chance for a random fit of a series of 20 intervals between the identified events with a combined error of 20 years and a mean recurrence of 100 years is of the order 10^{-10} (additional matching the six masked events by accident is even less likely). The best-fit curve was slightly shifted to the left of the radiocarbon ages, mostly by 50–200 years, with one exception of 350 years. This shift is reasonable because the Ein Gedi site is located within the deeper lacustrine environment. The small discrepancy between radiocarbon ages and the counting-model ages in the Ein Gedi core can be attributed to reworking of the washed-in organic matter before it settled in the

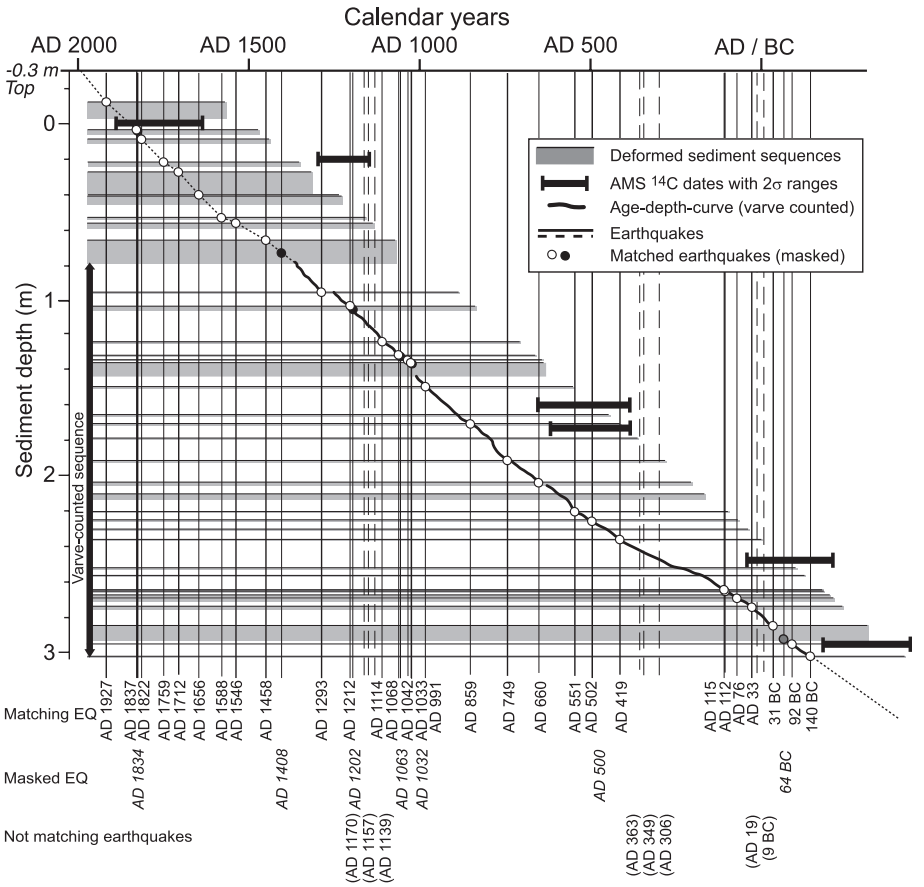

Fig. 4. The age-depth model of the Ein Gedi profile is derived from radiocarbon dating (black bars indicate 2ó ranges) and varve-counting between 0.78 and 3.03 m. The floating annual chronology is anchored by a systematic comparison and correlation of deformed sediment sequences (grey bars) to a succession of historical strong earthquakes.

bottom of the dense saline lake. This re-deposition effect shows lower values in the Ze'elim section [16] situated closer to the paleo-shoreline. There, eight historical seismic events were matched with radiocarbon dating within one sigma [32]. The slightly longer residence time inferred in the current study may also reflect the tighter constraints provided by comparison to a larger number of seismites and a very rigorous chronological framework.

The disturbed sequences are classified to three thickness types: Types I, II and III with respective thickness of >5, 1–5, and <1 cm, the latter identified only microscopically, hence restricted to the counted interval. The seismites outside the counted interval are identified by bare-eye examination of the core. For estimating recurrence intervals in the entire core, we therefore use only macroscopically observable seismites (Types I and II). Our choice of the absolute chronological matching for the counted interval (Fig. 4) anchors the chronology of the rest of the entire Ein Gedi core. Out of the 53 disturbed sequences in the 21 m core, 31 can be correlated with historical earthquakes along the last three millennia. Additional eight seismites can be matched with the less well-constrained archeoseismic record, totalling 39 deformed sequences matched by independent records.

The uppermost-disturbed layer corresponds to the A.D. 1927 earthquake [10,12,13,33,34], which is consistent with the sedimentation rate, the top of the profile representing the year A.D. 1997. The whole match encompasses the past 2760 years (the upper 3.70 m of the core). Although historical documentary

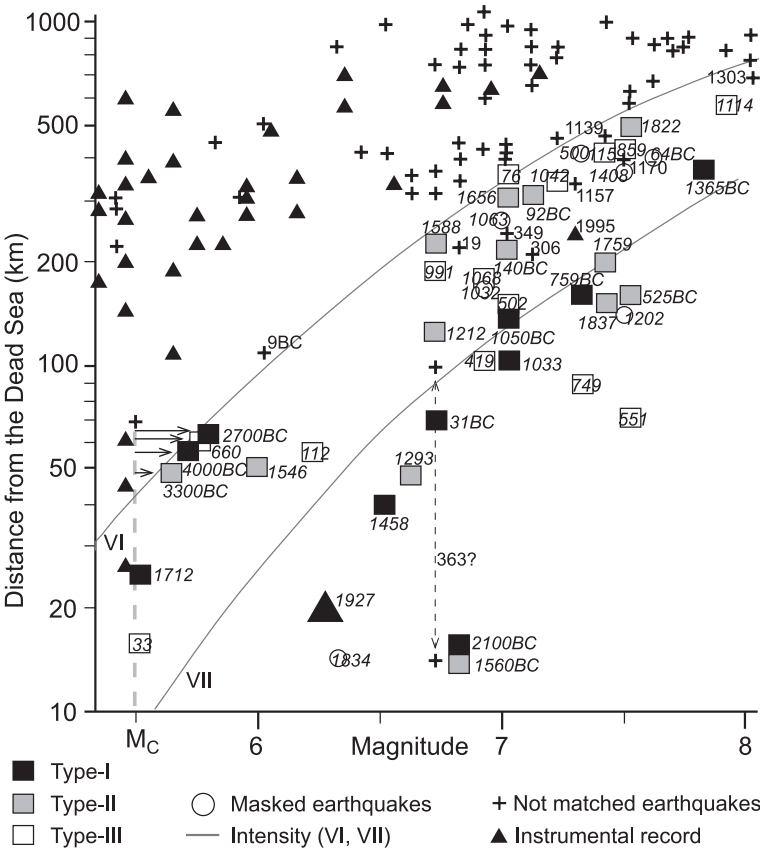

Fig. 5. All available magnitudes of historical earthquakes for a distance of up to 1000 km around the Dead Sea on a logarithmic scale. The correlated earthquakes (squares) plot into a field of intensities greater than VI (dashed line); beyond the intensity VII, all earthquakes are correlated (except the A.D. 363 earthquake—see text). Uncorrelated historical events are represented by a cross (for historical record) and a triangle (for instrumental record). The instrumental measurements are possible since 100 years [11]. According to some matching historical earthquakes with an unknown magnitude, a critical magnitude $M_C = 5.5$ is necessary to develop a disturbed sediment sequence.

records prior to this period do not exist, radiocarbon dated archaeological evidence has enabled us to further extend the seismic record to ~6000 years [4,35]. Moreover, the Ein Gedi core exposes additional disturbed sequences that are still older (Table 2 and Fig. 6A).

The spatial distribution of deformation in the Dead Sea sediments can be examined by comparison of the chronology of the Ein Gedi core to the other sites along the Dead Sea shore. The Ein Feshkha core (Fig. 2) recovered some of the same period represented in Ein Gedi core, albeit with a lower quality and with over 10 coring discontinuities. Nevertheless, with the available chronological information, all 18 disturbed sequences identified in the Ein Feshkha core coincide with seismites in the Ein Gedi core. Most of the events missing in Ein Feshkha core but found in Ein Gedi core happened during periods of hiatus in the former, including 13 in the last 800 years (Fig. 2). The older disturbances of the Ein Gedi record (~5000–6000 and 6000–6800 B.C.) can be correlated with deformed units of the Darga valley sedimentary record [29]. All eight earthquakes found previously in the Ze'elim terrace [16], can be identified in the Ein Gedi core. With some reasonable modifications, the agreement between the correlated sections is also substantiated in details. The two liquefied sand structures at Ze'elim, representing the earthquakes of A.D. 1927 and 1834 [16], are correlated with very thick disturbed sequences in the Ein Gedi core. Here we allow the

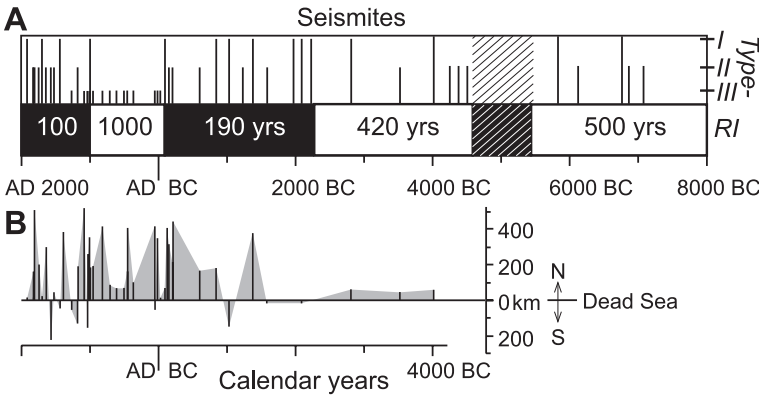

Fig. 6. (A) Classification of disturbed sediment sequences into three types based on thickness. The recurrence interval (RI) can be estimated from the temporal distribution of Type-I and -II seismites, with one exception between 4500 and 5500 B.C. Within this sequence, the macroscopical identification of seismites is delicate because of altered sediment characteristics. (B) North–South distribution of the epicenters of the matched earthquakes.

possibility that the correlated earthquake at both sites is the A.D. 1837 event rather than the A.D. 1834 earthquake. In this interpretation the A.D. 1834 is masked by the later event, which in turn is documented as a strong earthquake originating close to Safed [13,27]. Further, very thin sequences exist at both sites, reflecting the earthquakes of A.D. 419 and 33, and 64 B.C. The correlation of the A.D. 363 earthquake [16] was changed in favor of the A.D. 419 event at the Ze'elim profile, without any contradiction of the former results. In addition, a relatively thick sequence representing the event of 31 B.C., shows similar appearance in both sections. The identification of A.D. 363 was based on a catalogue [13] inferring a large event for this year without support of historical sources for rupture south of Beit Shean (Skithopolis; 32°30′ N). Rather, reported damage in the Galilee dated to this year was compiled with archaeological damage in Petra, south of the Dead Sea, dated to within a decade [35].

The magnitudes of all strong earthquakes in relation to their distance from the Dead Sea [27,36] as shown in Fig. 5 were calculated from local intensities according to former studies [10,13]. It appears that the local intensity exerts a dominant control on the formation of seismites. At historically estimated intensities greater than VII, all earthquakes (with the exception of the debatable A.D. 363 event) are matching, whereas at intensities smaller than VI none are matching. About 60% of the correlated earthquakes that plot in the intermediate range are correlated. These results corroborate both the historical magnitude and location estimates, albeit imprecise.

We find no correlation between seismite type (or thickness) and calculated intensity. This suggests that seismite generation is hysteretic, so once a threshold of energy is exceeded, an undetermined fraction of that energy can go to suspension and mixing of the sediment.

4. Temporal distribution of the Holocene seismites

We can use only the deformed sequences of Types I and II for analyzing the recurrence pattern of seismites along most of the core, because the identification of Type-III events is restricted to the counted interval. Within the span of the last 1000 years, ten disturbed sequences could be identified (additionally 3 of Type-III), representing a mean recurrence interval of 100 years. For the 1st Millennium (A.D. 0–1000) only a single seismite of Type-I is identified, so the recurrence interval changes to ~1000 years. Between 0 and 2100 B.C. six events of Type-I, and five events of Type-II can be identified. Here, the mean recurrence interval is approximately 190 years, whereas during 2100–4600 B.C. only two of Type-I and four of Type-II can be found, with the corresponding recurrence interval of 420 years. The section from 4600 to 5500 B.C. was excluded from the evaluation

because of the lithological characteristic of this interval: Our means to identify disturbed sequences requires the presence of alternating aragonite and clastic laminae, while this interval contains mainly clastic sediments, with a few aragonite laminae. Two disturbed sequences of Type-I, and three of Type-II, lead to a recurrence interval of 500 years for the oldest part of the core, between 5500 and 8000 B.C.

Overall, the recurrence data from the Dead Sea suggest that the rate of seismic activity along the DST changed several times during the last 10,000 years: There is a very active period within the past 500–600 years, whereas between 1000 and 2000 years ago the seismic activity was significantly less frequent. The pre-historical time span between 0 and 4600 B.C. shows moderate seismicity, with a sub-clustering at 1000–2100 B.C. The lack of disturbed sequences in the lower part of the Ein Gedi profile (5500–8000 B.C.) indicates a relatively quiet time for seismic activity (Fig. 6A).

Considering also the microscopically observed Type-III seismites in the counted interval (140 B.C.–A.D. 1458), a quiescent period between A.D. 551 and 1033 is obvious. A similar relatively quiet period (A.D. 520–940) was reported before for the North Anatolian Fault (NAF), whilst by contrast a cluster of frequent seismic activity along the East Anatolian Fault was observed [3]. The similarity in the behavior of the NAF and the Dead Sea Transform and their dissimilarity to the intervening EAF is discussed in Section 5 below.

Data of epicentral distance to farthest liquefaction versus seismic moment have been complied for over a hundred modern shallow focus earthquakes [36]. Thereby an envelope of maximum distance for a given moment-magnitude was inferred (Intensity VII

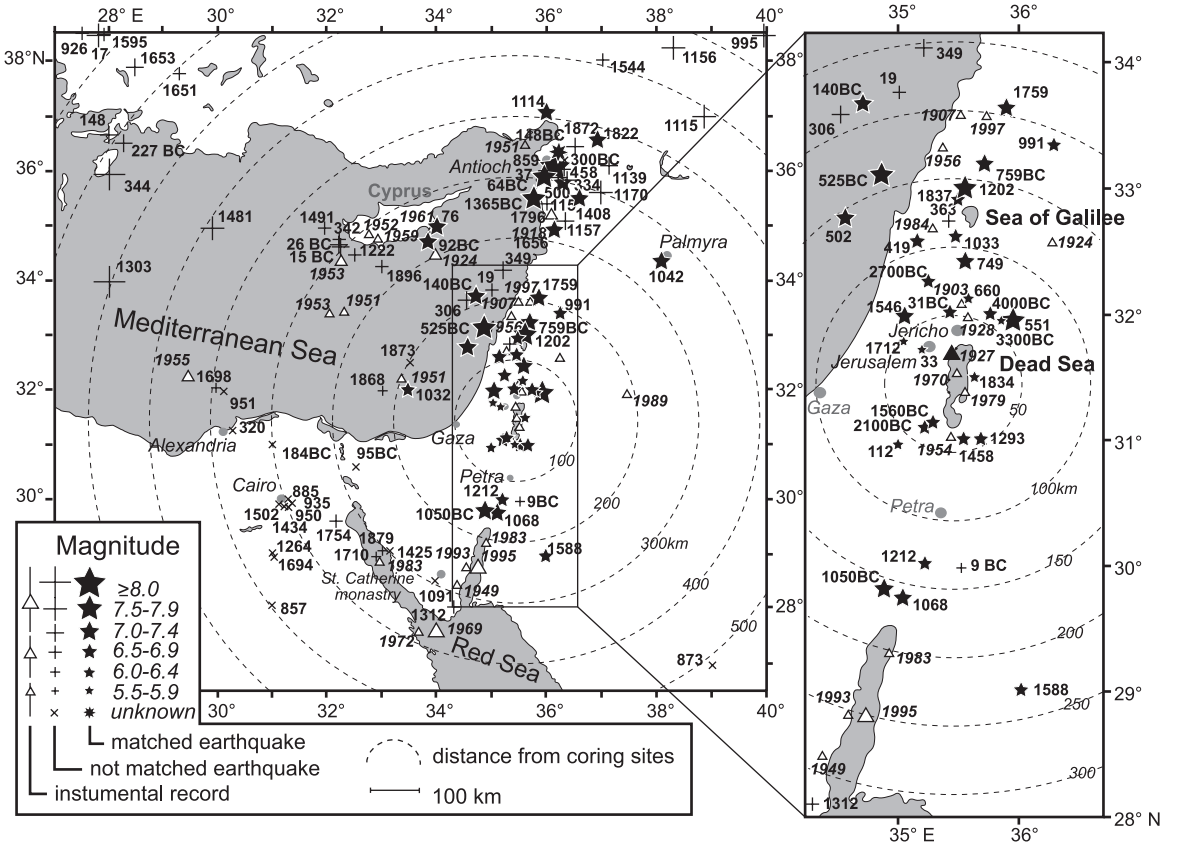

Fig. 7. Map of severe (M_L>5.5) earthquakes in the Eastern Mediterranean and the Dead Sea region; correlated earthquakes (stars), and not matching instrumental (triangles) and historical record (crosses).

in Fig. 5). The intermediate intensity range ($VI < I_0 < VII$) highlights the limitations of the present method and of the historical intensity estimate (based on location and magnitude determinations).

Nevertheless, some older events with unknown magnitude (4000, 3300 and 2700 B.C. and A.D. 660) which all match to the age-depth model, can now be assessed more precisely. We calculated their magnitude according to the distance of their epicenters from the Dead Sea in Fig. 5. The fact that they all can be matched is consistent with a minimum intensity of VI. In addition a certain threshold magnitude of $\sim 5.5–6.0$ seems to be essential for creating a disturbed sequence in the sediment [7].

With a few exceptions, the epicenters of the matched earthquakes are situated very close to the Dead Sea (within 150 km) or up to 500 km north of it along the DST (Fig. 7). Between 1050 B.C. and A.D. 1000, and from A.D. 1600 to recent time the epicenters are all located along the northern segment of the DST, whereas prior to 1050 B.C. and between A.D. 1000 and 1600 they appear to scatter along several earthquake rupture segments of the DST (Fig. 6B). This observation may be sensitive to the distribution of settlements, as well as to the particular location of the core along the western boundary of the Dead Sea pull-apart, the one that continues to the north.

5. Comparison between seismic activity along the DST and the Anatolian faults

The core data provide a means to evaluate the timing of rupture events along the major plate boundaries in the region; the chronology of events can be further applied for understanding of the broad scale elastic coupling. The information from the Dead Sea sediments can be combined with historical catalogues and excavations of fault traces for recovering the actual energy and seismic moment release, which are currently in progress [8,28,30]. As discussed by Marco et al. [7], clustering of earthquakes in time may bias the estimate of slip rate based on short-term seismic moment release. The present study reaffirms this both by corroborating the seismic nature of disturbed layers, and by showing clustering over the millennial time scale. Nonetheless, we can compare variations in seismicity rate in the earthquake chronology recovered from the Dead Sea sediments with data from adjacent plate boundaries. Fig. 8 displays cumulative earthquake number versus years recorded in the Ein Gedi core together with historical data from the Anatolian faults. While the data does not detail the size of the earthquake, an interesting correlation is apparent. The record clearly shows that the strong earthquakes expressed by the sedimentary structures in the core are closely linked with the DST suggesting temporal changes in locus of main seismic activity along this fault. On a regional scale, both the DST and the East Anatolian Fault (EAF) transform tectonic displacement to the southern boundary of the Eurasian Plate (Fig. 1). This boundary includes the North Anatolian Fault (NAF) along which the Anatolian continental block escapes westward [6,37]. The long-standing suggestion of Ambraseys [3] regarding alternation of seismic activity between the EAF and the NAF [3,31] is echoed in this study by the paleoseismic record of the DST (Fig. 8). During the 1st Millennium, it appears that the activity along NAF is in tandem with the DST and both alternate with the EAF: Between A.D. 500 and 1000 NAF and DST are quiescent whereas EAF is active; the converse is observed before A.D. 500 (Fig. 8).

Alternating activity along 10^3 km scale boundaries over periods of several hundred years suggests broad-scale elastic coupling: The alternation of activity between the NAF/DST and EAF has been discussed

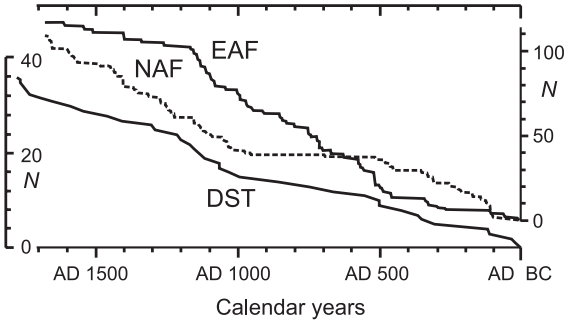

Fig. 8. Cumulative number of severe earthquakes shown for A.D. 0–1700; the data from EAF and NAF according to Hubert-Ferrari et al. [31]. The comparison with available data of earthquakes generated along the DST reveals the similarity between DST and NAF, and the dissimilarity to EAF within A.D. 0–900, and the similarity between DST and EAF within A.D. 900–1700.

in the context of the evolution of the fault system [37]. Elastic modeling suggests that activities on the two branches of the Anatolian Block are mutually exclusive. However, after slip propagates through the EAF, this boundary becomes inactive, and elastic strain is released by slip on the NAF.

Accordingly, the westward extrusion of the Anatolian block by motion along the mutually locking Anatolian fault system is eased by the alternation of seismicity. Therefore broad scale elastic coupling between DST and NAF may illustrate the mechanism underlying lateral extrusion (escape) tectonics typical for continental plate collision. This concept can be tested by on-fault studies that will give better constraints on each of the ruptures that caused brecciation in the Dead Sea sediments [8,28,30].

Acknowledgements

Financial support by the German-Israeli Foundation for Scientific Research and Development (GIF) is gratefully acknowledged. *[VC]*

References

[1] S. McClusky, S. Balassanian, A. Barka, C. Demir, S. Ergintav, I. Georgiev, O. Gurkan, M. Hamburger, K. Hurst, H. Kahle, K. Kastens, G. Kekelidze, R. King, V. Kotzev, O. Lenk, S. Mahmoud, A. Mishin, M. Nadariya, A. Ouzounis, D. Paradissis, Y. Prilepin, M. Prilepin, R. Reilinger, I. Sanli, H. Seeger, A. Tealeb, M.N. Tokzöz, G. Veis, Global positioning system constraints on plate kinematics and dynamics in the eastern Mediterranean and Caucasus, J. Geophys. Res. 105 (B3) (2000) 5695–5719.

[2] Z. Garfunkel, I. Zak, R. Freund, Active faulting in the Dead Sea Rift, Tectonophysics 80 (1981) 1–26.

[3] N.N. Ambraseys, Value of historical records of earthquakes, Nature 232 (1971) 375–379.

[4] I. Karcz, U. Kafri, Z. Meshel, Archaeological evidence for subrecent seismic activity along the Dead Sea-Jordan rift, Nature 269 (1977) 234–235.

[5] R.G. North, Seismic slip rates in the Mediterranean and Middle East, Nature 252 (1974) 560–563.

[6] D. Kempler, Z. Garfunkel, Structures and kinematics in the northeastern Mediterranean: a study of an irregular plate boundary, Tectonophysics 234 (1994) 19–32.

[7] S. Marco, M. Stein, A. Agnon, H. Ron, Long-term earthquake clustering: a 50,000-year paleoseismic record in the Dead Sea Graben, J. Geophys. Res. 101 (1996) 6179–6191.

[8] Y. Klinger, J.P. Avouac, N. Abou-Karaki, L. Dorbath, D. Bourles, J.L. Reyss, Slip rate on the Dead Sea transform fault in northern Araba valley (Jordan), Geophys. J. Int. 142 (2000) 755–768.

[9] S. Wdowinski, Y. Bock, G. Baer, L. Prawirodirdjo, N. Bechor, S. Naaman, Knafo, Y. Forrai, Y. Melzer, GPS Measurements of Current Crustal Movements along the Dead Sea Fault, J. Geophys. Res. (in press).

[10] A. Salamon, A. Hofstetter, Z. Garfunkel, H. Ron, Seismotectonics of the Sinai subplate—the eastern Mediterranean region, Geophys. J. Int. 155 (2003) 149–173.

[11] D. Neev, K.O. Emery, The Destruction of Sodom, Gomorrah, and Jericho, Oxford Univ. Press, New York, 1995. 163 pp.

[12] N.N. Ambraseys, C.P. Melville, R.D. Adams, The Seismicity of Egypt, Arabia and the Red Sea: A Historical Review, Cambridge Univ. Press, Cambridge, UK, 1994. 181 pp.

[13] D.H.K. Amiran, E. Arieh, T. Turcotte, Earthquakes in Israel and adjacent areas: macroscopic observations since 100 B.C.E., Isr. Explor. J. 44 (1994) 260–305.

[14] E. Guidoboni (Ed.), Catalogue of Ancient Earthquakes in the Mediterranean Area Up to the 10th Century, Istituto nazionale di geofisica, Rome, 1994. 504 pp.

[15] A. Ben-Menahem, Four thousand years of seismicity along the Dead Sea Rift, J. Geophys. Res. 96 (1991) 20195–20216.

[16] R. Ken-Tor, A. Agnon, Y. Enzel, M. Stein, S. Marco, J.F.W. Negendank, High-resolution geological record of historic earthquakes in the Dead Sea basin, J. Geophys. Res. 106 (2001) 2221–2234.

[17] R. Bookman (Ken-Tor), Y. Enzel, A. Agnon, M. Stein, Late Holocene lake levels of the Dead Sea, GSA Bulletin (in press).

[18] Y. Yechieli, M. Magaritz, Y. Levi, U. Weber, U. Kafri, W. Woelfli, G. Bonani, Late Quaternary geological history of the Dead Sea area, Israel, Quat. Res. 39 (1993) 59–67.

[19] M. Stein, A. Starinsky, A. Katz, S.L. Goldstein, M. Machlus, A. Schramm, Strontium isotopic, chemical, and sedimentological evidence for the evolution of Lake Lisan and the Dead Sea, Geochim. Cosmochim. Acta 61 (1997) 3975–3992.

[20] M. Stuiver, P.J. Reimer, E. Bard, J.W. Beck, G.S. Burr, K.A. Hughen, B. Kromer, G. McCormac, J. Van der Plicht, M. Spurk, INTCAL98 radiocarbon age calibration, 24,000–0 cal BP, Radiocarbon 40 (1998) 1041–1083.

[21] S. Prasad, J.F.W. Negendank, M. Stein, Late Pleistocene palaeoclimate record from palaeolake Lisan, Israel, Eos Trans. AGU 82 (2001) 784.

[22] Z.H. El-Isa, H. Mustafa, Earthquake deformations in the Lisan deposits and seismotectonic implications, Geophys. J. R. Astron. Soc. 86 (1986) 413–424.

[23] Z.B. Begin, A. Ehrlich, Y. Nathan, Lake Lisan, the Pleistocene precursor of the Dead Sea, Bull.-Isr. Geol. Surv. 63 (1974) 33.

[24] A. Katz, Y. Kolodny, A. Nissenbaum, The geochemical evolution of the Pleistocene Lake Lisan-Dead Sea system, Geochim. Cosmochim. Acta 41 (1977) 1609–1626.

[25] S. Marco, A. Agnon, Prehistoric earthquake deformations near Masada, Dead Sea graben, Geology 23 (1995) 695–698.

[26] A. Schramm-Haase, S.L. Goldstein, M. Stein, U–Th disequilibrium dating of Lake Lisan aragonite (late Pleistocene Dead

Sea) and implications for glacial East Mediterranean climate change, Geochim. Cosmochim. Acta 68 (2004) 985–1005.
[27] N.N. Ambraseys, J.A. Jackson, Faulting associated with historical and recent earthquakes in the Eastern Mediterranean region, Geophys. J. Int. 133 (1998) 390–406.
[28] R. Ellenblum, S. Marco, A. Agnon, T. Rockwell, A. Boas, Crusader castle torn apart by earthquake at dawn, 20 May 1202, Geology 26 (1998) 303–306.
[29] Y. Enzel, G. Kadan, Y. Eyal, Holocene earthquakes inferred from a Fan-Delta sequence in The Dead Sea Graben, Quat. Res. 53 (2000) 34–48.
[30] M. Meghraoui, F. Gomez, R. Sbeinati, J. Van der Woerd, M. Mouty, A. Nasser Darkal, Y. Radwan, I. Layyous, H. Al Najjar, R. Darawcheh, F. Hijazi, R. Al-Ghazzi, M. Barazangi, Evidence for 830 years of seismic quiescence from palaeoseismology, archaeoseismology and historical seismicity along the Dead Sea fault in Syria, Earth Planet. Sci. Lett. 210 (2003) 35–52.
[31] A. Hubert-Ferrari, G.C.P. King, I. Manighetti, R. Armijo, B. Meyer, P. Tapponnier, Long-term elasticity in the continental lithosphere; modelling the Aden ridge propagation and the Anatolian extrusion process, Geophys. J. Int. 153 (2003) 111–132.
[32] R. Ken-Tor, M. Stein, Y. Enzel, A. Agnon, S. Marco, J.F.W. Negendank, Precision of calibrated radiocarbon ages of historic earthquakes in the Dead Sea basin, Radiocarbon 43 (2001) 1371–1382.
[33] T. Niemi, Z. Ben-Avraham, Evidence for Jericho earthquakes from slumped sediments of the Jordan River delta in the Dead Sea, Geology 22 (1994) 395–398.
[34] Z. Reches, D.F. Hoexter, Holocene seismic and tectonic activity in the Dead Sea area, Tectonophysics 80 (1981) 235–254.
[35] K.W. Russell, The earthquake chronology of Palestine and northwest Arabia from the 2nd through the mid-8th century A.D., Bull. Am. Sch. Orient. Res. 260 (1985) 37–59.
[36] N.N. Ambraseys, Engineering seismology, Earthquake Eng. Struct. 17 (1988) 1–105.
[37] J. Chorowicz, D. Dhont, N. Gündogdu, Neotectonics in the eastern North Anatolian fault region (Turkey) advocates crustal extension: mapping from SAR ERS imagery and Digital Elevation Model, J. Struct. Geol. 21 (1999) 511–532.